SLAC-100
UC-37
(ACC)

DIGITAL COMPUTER ERROR ANALYSIS OF A RESONANT TOROID CHARGE MONITOR

DALE HORELICK AND RAYMOND S. LARSEN

STANFORD LINEAR ACCELERATOR CENTER

STANFORD UNIVERSITY

Stanford, California

PREPARED FOR THE U.S. ATOMIC ENERGY

COMMISSION UNDER CONTRACT NO. AT(04-3)-515

March 1969

ABSTRACT

A mathematically exact error analysis is performed on an ideal resonant toroid charge monitor for varying beam pulse width, assuming calibration with a known impulse charge. An optimum waveform sampling point is derived from the data, which minimizes the error. The effects of using a rectangular calibration pulse are analyzed, and the error for an impulse beam is calculated as a limiting case of beam charge distribution. Errors for variation in system timing are also analyzed.

All computations are performed on a digital computer to obtain the required precision. The results show that a maximum error of ± .012% can be achieved over a pulse width range of 0-2 μsec, with a resonant frequency of 5.25 kHz and a damping time constant of 0.33 msec. Under the same conditions the maximum timing error is about - 0.07%/μsec.

ACKNOWLEDGMENTS

The authors gratefully acknowledge the computer programming support provided by Dr. A. Barna and Mrs. A. Johnson.

TABLE OF CONTENTS

LIST OF FIGURES

I. INTRODUCTION

In a toroidal charge monitoring system currently in use at SLAC, the beam pulse* charge is measured to an accuracy of ± 0.1% using a resonant technique. In a previous report on this system[1] an error analysis of the resonant toroid is performed based on certain simplifying assumptions. However, the errors inherent in the mathematical approximations are comparable to the effects being investigated, and a more exact analysis is warranted. The present paper describes an error analysis of the resonant toroid circuit model, using a digital computer, in which the effects of varying beam pulse width and system timing instabilities are analyzed.

All calculations were performed on an IBM 360 computer using Fortran IV language. Due to the nature of the calculations it was found that double precision arithmetic was necessary to achieve the desired accuracy. The error curves, except for a few interpolated from others, are plotted directly from the computer output; hence they are mathematically exact within the limits of plotting.

II. CHARGE MONITOR SYSTEM

The system and associated waveforms are shown in Fig. 1. The operation is described briefly as follows:

Passage of a beam pulse through the toroid causes a charge to accumulate on a capacitor connected across the toroid terminals. The toroid-capacitor system then oscillates, the peak amplitude of the damped oscillation being very nearly proportional to the amount of beam charge. Using a precise beam pretrigger as a timing reference, the amplified signal is sampled near the second peak, converted into a digital number, and added into a digital accumulator; the accumulator thus displays the total charge passing through the toroid over a period of time.

The basis for system accuracy is a calibration system capable of simulating beams of precisely 10^{-8}, 10^{-9} or 10^{-10} coulombs per pulse. The shape of the calibration pulse is approximately triangular with a half-maximum width of less than 0.5 μsec. Using this pulse, sample point timing and system gain are adjusted very precisely.

---

*The SLAC beam characteristics are: pulse width, 0.2 to 2 μsec; shape, approximately rectangular; maximum peak amplitude, 50 mA; rate, up to 360 pps in multiples of 60 pps; type of particles, electrons or positrons.

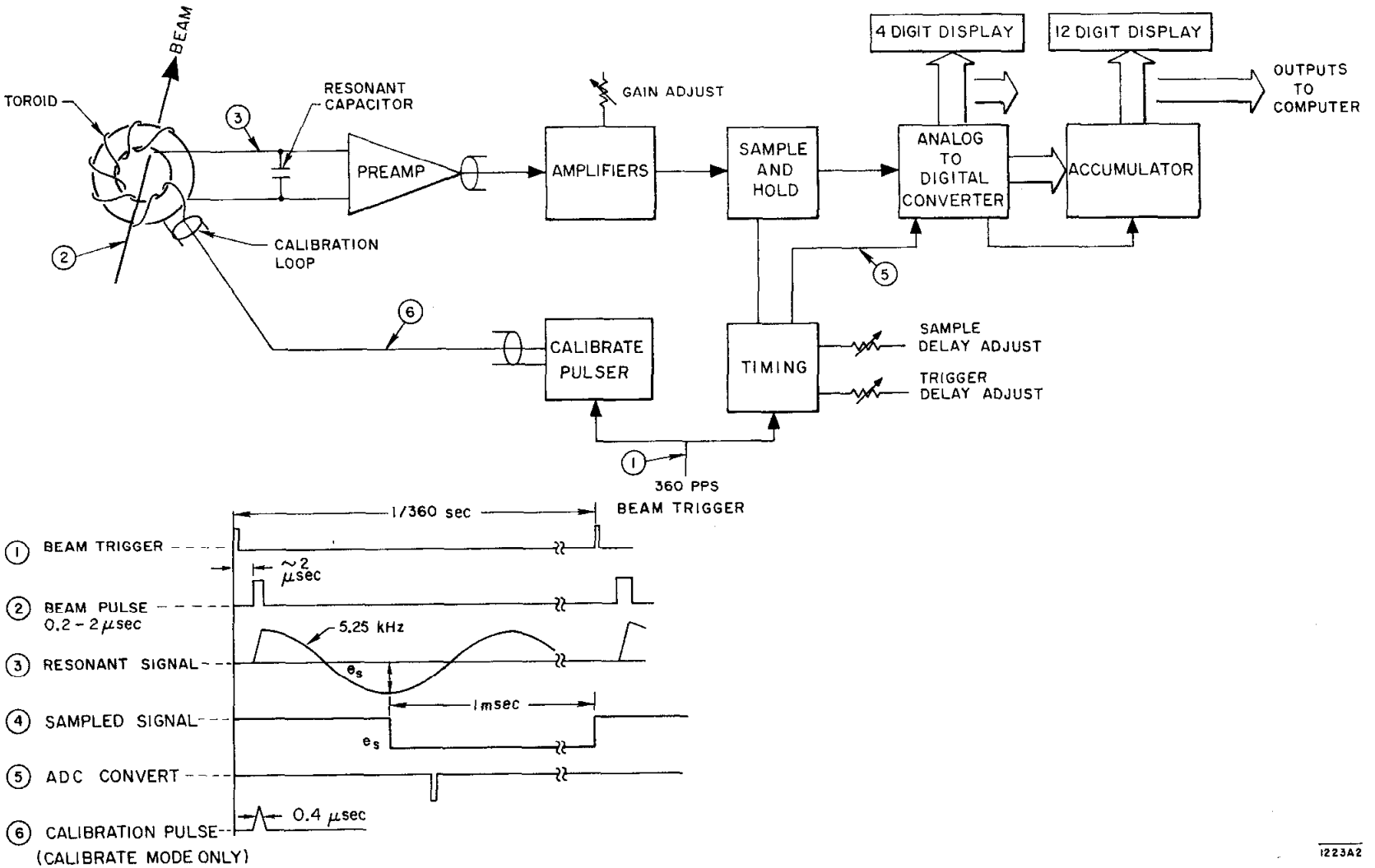

FIG. 1--Resonant toroid charge monitor system and waveforms.

III. THE RESONANT TOROID MODEL

Figure 2 shows the circuit model used for the resonant toroid. The toroid is assumed to be an ideal current transformer, with the beam equivalent to an ideal current source driving a single turn primary.[2,3] Coil resistance and inter-turn capacitance are neglected, but core losses and stray capacitance are a part of R and C respectively. Resistance R also represents the input impedance to the preamplifier, in parallel with a separate damping resistor. Positional effects of the beam[4] are neglected in this model.

The circuit values used in the actual system, which are referred to later in this report, are as follows:

$$L = 28 \text{ mH} \qquad C = .033\ \mu\text{F} \qquad R = 5000\Omega \qquad f_0 = 5.25 \text{ kHz}$$

The beam current pulse is assumed to be rectangular, and the spacing between pulses large enough so that there is no interpulse error between successive beam pulses — i.e., the damping time constant is much shorter than the interpulse period.

Using this model, Laplace transform methods will be used to determine the output voltage transient. For a generalized current input, I(t),

$$e_0(s) = \frac{I(s)}{Y(s)} = I(s)\ \frac{sL}{1 + s\frac{L}{R} + s^2 LC} \tag{1}$$

For a rectangular current pulse input of amplitude I_b/N and width T

$$I(s) = \frac{I_b}{N}\frac{1}{s}(1 - e^{-sT}) \tag{2}$$

Then

$$e_0(s) = \frac{I_b}{NC}(1 - e^{-sT})\ \frac{1}{s^2 + \frac{s}{RC} + \frac{1}{LC}} \tag{3}$$

For $\left(\frac{1}{2RC}\right)^2 - \frac{1}{LC} < 0$ this transform has the resonant form of solution for $e_0(t)$:

$$e_0(t) = \frac{I_b}{NC\omega_0}\, e^{-t/2RC}\left[\sin \omega_0 t - e^{T/2RC} \sin \omega_0(t-T)\, u(t-T)\right] \tag{4}$$

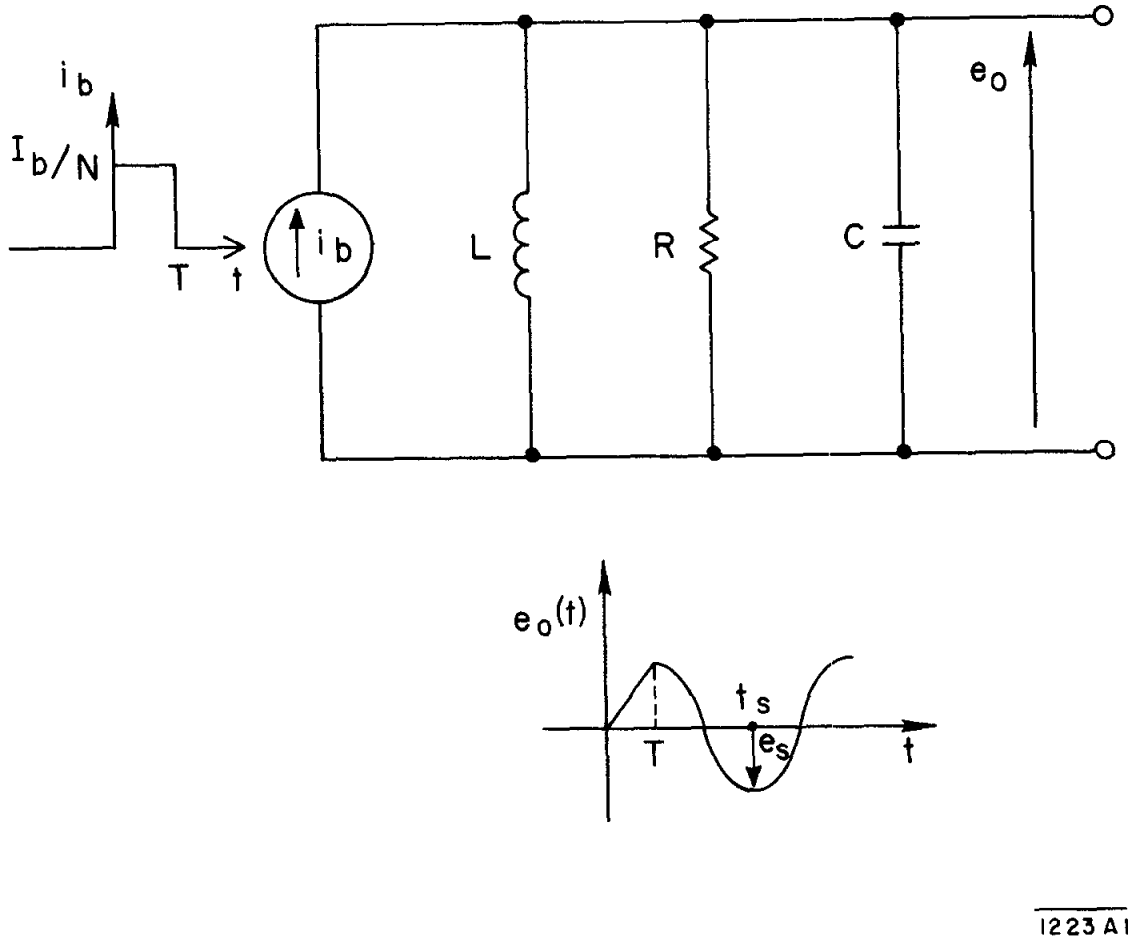

FIG. 2--Resonant toroid circuit model.

The resonant angular frequency, $\omega_0 = 2\pi f_0$, is given by

$$\omega_0 = \sqrt{\frac{1}{LC} - \frac{1}{(2RC)^2}} \tag{5}$$

When $T \ll 2RC$ and $T \ll \frac{1}{\omega_0}$, $e_0(t)$ has the general form shown in Fig. 2.

IV. DEVELOPMENT OF THE PULSE WIDTH ERROR EQUATION

The amplitude of $e_0(t)$ can be shown to be approximately proportional to the total charge in the current pulse. Assume that $T \ll \frac{1}{\omega_0}$, and $T \ll 2RC$. Then approximating $e^{T/2RC} \to 1$, $\sin \omega_0 T \to \omega_0 T$, and $\cos \omega_0 T \to 1$,

$$e_0(t) \cong \frac{I_b T}{NC} e^{-t/2RC} \cos \omega_0 t \tag{6}$$

The term $I_b T$ is exactly the charge Q in the rectangular current pulse so that

$$e_0(t) \cong \frac{Q}{NC} e^{-t/2RC} \cos \omega_0 t \tag{7}$$

If the waveform is measured or sampled at t_s then $e_s \cong KQ$ where $K = \frac{e^{-t_s/2RC} \cos \omega_0 t_s}{NC}$. It is most practical to measure the waveform near the peak in the vicinity of $\omega_0 t_s = \pi$, since the waveform slope is near zero, minimizing sampling errors, and is well removed from the effects of any secondary beam disturbances.

Substituting $Q = I_b T$ into the exact Eq. (4) and replacing t by the sampling time t_s yields the sampled voltage e_s:

$$e_s = \frac{Q}{NC\omega_0 T} e^{-t_s/2RC} \left[\sin \omega_0 t_s - e^{T/2RC} \sin \omega_0 (t_s - T)\right], \tag{8}$$

valid for $t_s > T$.

The error analysis is based on the assumption of an ideal calibrator which injects a calibration impulse* charge into the toroid at t = 0, so that timing and

*An impulse calibration charge is defined as the passage of a precisely known charge in infinitesimal time.

gain can be accurately adjusted. Adjustment on an impulse results in zero theoretical error in measuring "zero width" beam pulses. The use of the calibrator compensates for slow changes in C, 2RC, and ω_0 so that these parameters may be considered known constants in the analysis.

In order to introduce the calibration charge into Eq. (8), the response to an impulse current must be found by applying L'Hospital's rule to Eq. (8) to find the limit as $T \to 0$.

$$e_s\Big|_{T\to 0} = \frac{Qe^{-t_s/2RC}}{NC}\left[\cos \omega_0 t_s - \frac{1}{2RC\,\omega_0}\sin \omega_0 t_s\right] \tag{9}$$

If $(e_s)_{cal}$ is the given calibration voltage for the calibration charge Q_{cal} then

$$\frac{e^{-t_s/2RC}}{NC} = \frac{(e_s)_{cal}}{Q_{cal}\left[\cos \omega_0 t_s - \frac{1}{2RC\,\omega_0}\sin \omega_0 t_s\right]} \tag{10}$$

Substituting Eq. (10) into Eq. (8),

$$e_s = \frac{Q}{\omega_0 T}\frac{(e_s)_{cal}}{Q_{cal}}\frac{\left[\sin \omega_0 t_s - e^{T/2RC}\sin \omega_0(t_s - T)\right]}{\left[\cos \omega_0 t_s - \frac{1}{2RC\,\omega_0}\sin \omega_0 t_s\right]} \tag{11}$$

If the relative error is defined as

$$\text{Error} = \frac{\text{Measured Charge - True Charge}}{\text{True Charge}}$$

or

$$\text{Error} = \frac{Q_{meas}}{Q} - 1 = e_s\,\frac{Q_{cal}}{(e_s)_{cal}} \times \frac{1}{Q} - 1 \tag{12}$$

then the final equation for the relative error is

$$\text{Error} = \frac{1}{\omega_0 T}\frac{\left[\sin \omega_0 t_s - e^{T/2RC}\sin \omega_0(t_s - T)\right]}{\left[\cos \omega_0 t_s - \frac{1}{2RC\,\omega_0}\sin \omega_0 t_s\right]} - 1 \tag{13}$$

This equation relates the charge measurement error to pulse width T, at a given sampling time t_s, assuming impulse charge calibration at t = 0. Since T is the variable parameter this error will be referred to as the pulse width error.

The parameters ω_0 and 2RC are characteristics of the electrical components, whereas t_s is a system parameter. Since the waveform is measured near the peak, the true peak for an impulse charge at t = 0 will be used as the reference point from which a small compensation angle θ_c is measured.*

V. LOCATION OF THE PEAK FOR AN IMPULSE CHARGE INPUT

In order to locate the peak of the waveform differentiate Eq. (9), the expression for the impulse response:

$$\left.\frac{de_s}{dt_s}\right|_{T\to 0} = \frac{Q}{NC}\left\{e^{-t_s/2RC}\left[-\omega_0 \sin \omega_0 t_s - \frac{1}{2RC}\cos \omega_0 t_s\right]\right.$$
$$\left. - \frac{1}{2RC}\, e^{-t_s/2RC}\left[\cos \omega_0 t_s - \frac{1}{2RC\ \omega_0} \sin \omega_0 t_s\right]\right\} = 0 \tag{14}$$

Let $t_s = t_p$ at the peak. Then from Eq. (14) it can be shown that

$$\tan \omega_0 t_p = \frac{4RC\ \omega_0}{1 - (2RC\ \omega_0)^2} \tag{15}$$

or

$$t_p = \frac{1}{\omega_0} \text{ arc tan } \frac{4RC\ \omega_0}{1 - (2RC\ \omega_0)^2}; \quad \frac{3\pi}{2\omega_0} > t_p > \frac{\pi}{2\omega_0} \tag{16}$$

The location of the peak, t_p, which is used in later computation can be calculated from the circuit parameters ω_0 and 2RC. Calculated values of t_p are given in Table 1, under two different conditions: (a) The damping time constant 2RC is held constant as the frequency ω_0 is varied, (b) the resistance R is held constant at 5000 ohms as ω_0 is varied with L held constant at 28×10^{-3} henries. In order to perform the latter calculations the required value of C is

---

*The term "compensation" is used since the offset from the peak tends to compensate for variation in pulse width, T, as shown in Section VI.A.

TABLE 1

LOCATION OF WAVEFORM PEAK

2RC (sec)	$\frac{\omega_0}{2\pi}$ (sec^{-1})	Impulse Cal Peak t_p (μsec)	Rectangular[2] Calibration Shift Δt_p (μsec)	Notes
$.330 \times 10^{-3}$	5.25×10^3	89.683890	.250082	2RC = .330 msec
$.330 \times 10^{-3}$	7.25×10^3	66.049150	.250072	
$.330 \times 10^{-3}$	9.25×10^3	52.261443	.250089	
$.330 \times 10^{-3}$	11.25×10^3	43.232198	.250079	
$.330 \times 10^{-3}$	13.25×10^3	36.861791	.250078	
$.330 \times 10^{-3}$	15.25×10^3	32.126976	.250082	
$.325395 \times 10^{-3}$	5.25×10^3	89.605717 See Note 1		R = 5 K (Constant) L = 28.0×10^{-3} H
$.169263 \times 10^{-3}$	7.25×10^3	63.302912		
$.102852 \times 10^{-3}$	9.25×10^3	48.350135		
$.068560 \times 10^{-3}$	11.25×10^3	38.686791		
$.048558 \times 10^{-3}$	13.25×10^3	31.910109		
$.035862 \times 10^{-3}$	15.25×10^3	26.875874		

[1]Note: The slight discrepancy between this figure and the first is due to the assumed value of L used to calculate C. This has no significant effect on the results since a self-consistent set of data was used.

[2]Rectangular calibration width of 0.5 μsec is assumed for this calculation.

found by rearranging the resonant frequency formula, Eq. (5):

$$C = \frac{1}{2\omega_0}\left[\frac{1}{\omega_0 L} + \sqrt{\frac{1}{(\omega_0 L)^2} - \frac{1}{R^2}}\right] \tag{17}$$

VI. PULSE WIDTH ERROR AS A FUNCTION OF RESONANT FREQUENCY

A. Error at $f_0 = 5.25$ kHz

The pulse width error equation (Eq. (13)) can be evaluated for $f_0 = 5.25$ kHz, $2RC = 0.330$ msec and T ranging from 0 to 2×10^{-6} sec. Selected values of t_s were used corresponding to a compensation angle, θ_c, ranging from -1° to 8°. The computed error is plotted in Fig. 3. As expected, the error is zero for an impulse ($T = 0$). For large compensation angles the error is positive, but for smaller angles, the error shows both positive and negative excursions over the range of T. Thus there is an optimum compensation angle in the vicinity of 1° which minimizes the peak absolute error. Further detail of the region around 1° with 0.1° resolution is shown in Fig. 4. Again, selecting the angle which minimizes the peak error yields an optimum angle of $1.05^\circ \pm .050^\circ$, the uncertainty being due to the resolution in θ_c. The peak error at this angle is about .012%. Note that the error at the optimum angle passes through zero at a beam width of 1.66 μsec.

B. Error for 2RC Constant

From Eq. (7), it may be seen that the toroid sensitivity, defined as e_{peak}/Q is approximately proportional to

$$\frac{e^{-t_p/2RC}}{C}$$

considering N to be a constant of the toroid. For $t_p \ll 2RC$, the peak amplitude then varies approximately as 1/C, or ω_0^2. Since it is desirable to maximize the sensitivity, it is important to evaluate pulse width errors for higher resonant frequencies.

The error calculations were repeated for the resonant frequencies of 7.25, 9.25, 11.25, 13.25 and 15.25 kHz, with the damping time 2RC held constant, a constraint which implies a change in both R and C as frequency varies, and

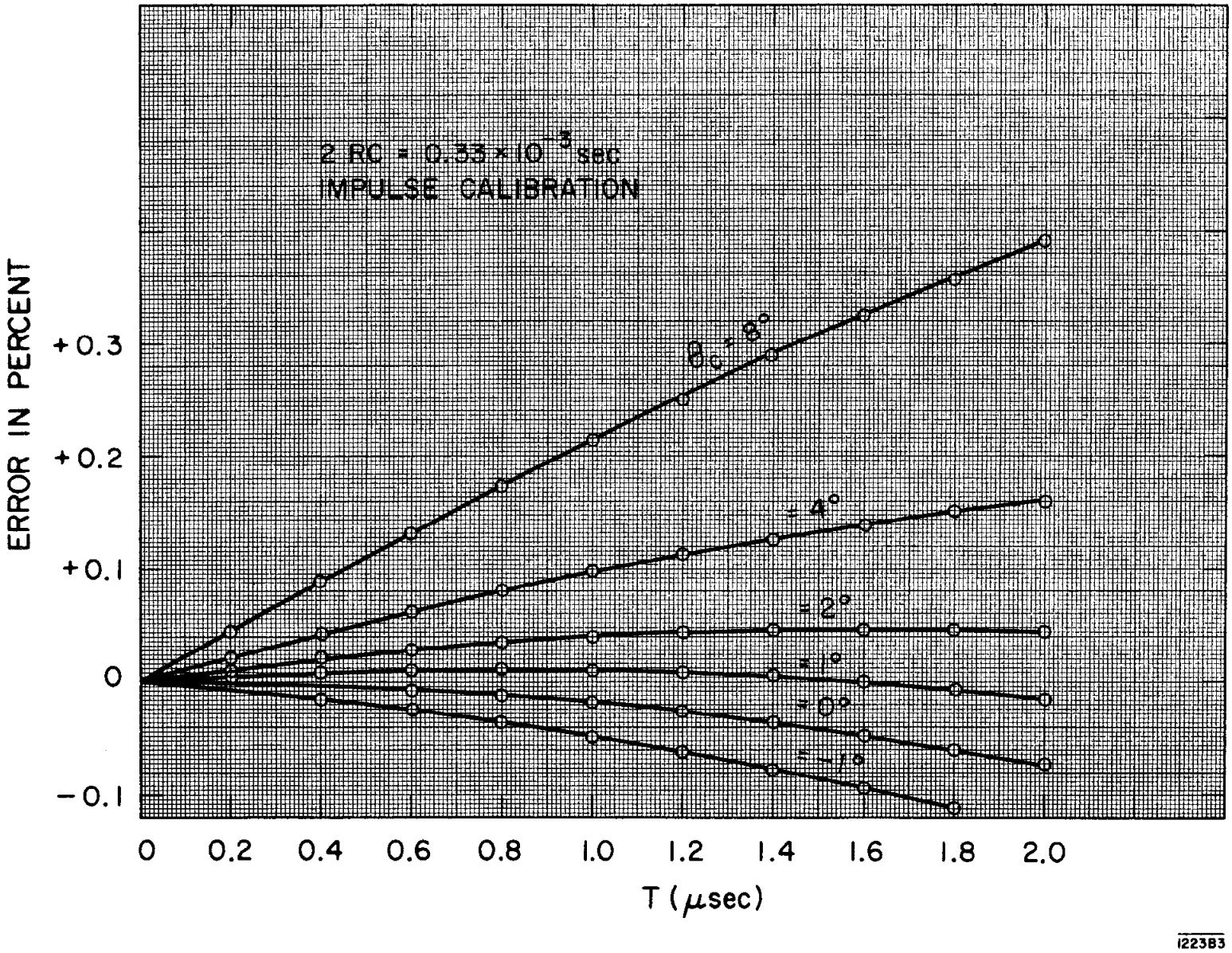

FIG. 3--Pulse width error at 5.25 kHz, θ_c ranging from -1° to $+8^{\circ}$.

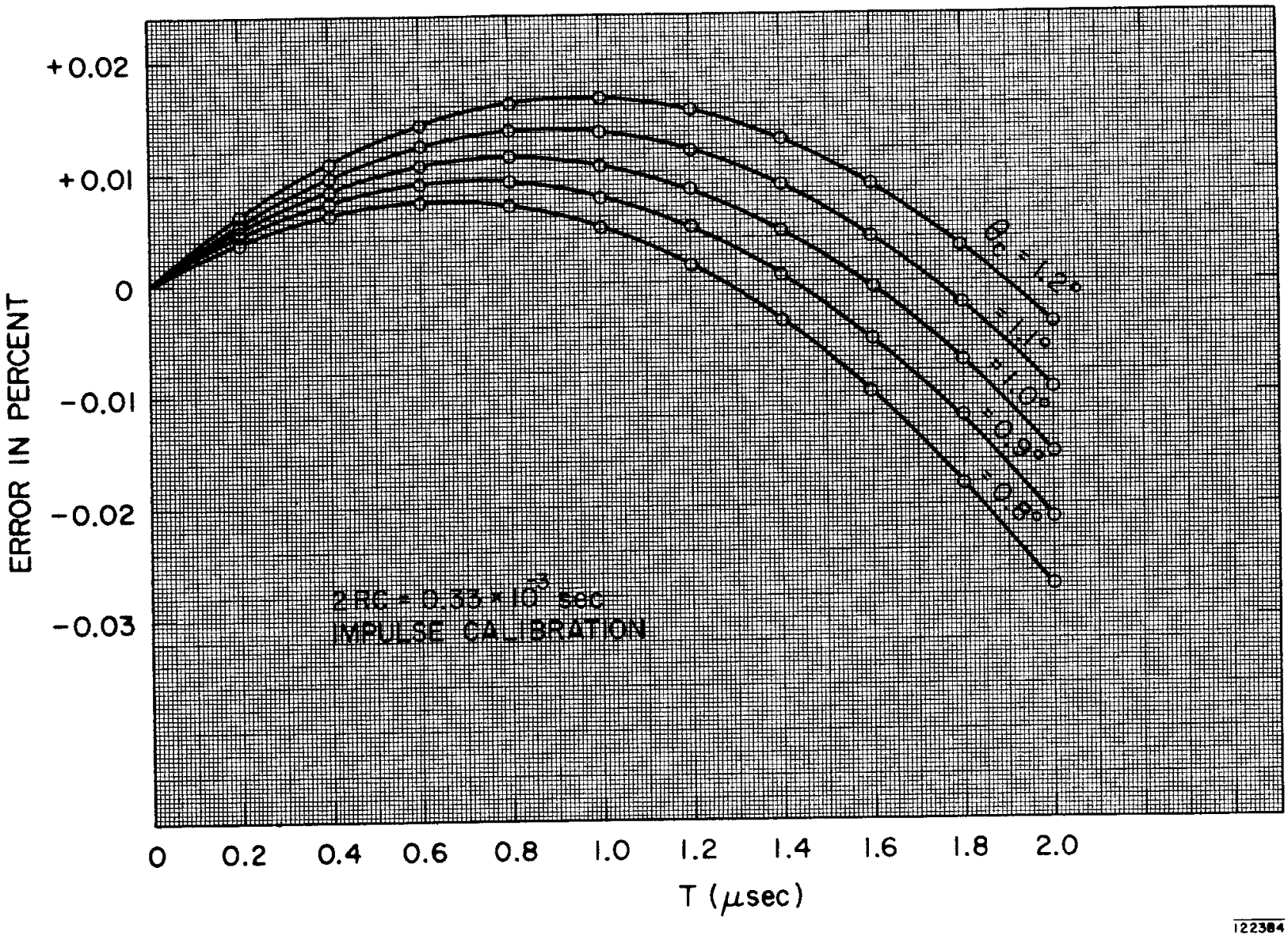

FIG. 4--Pulse width error at 5.25 kHz in vicinity of $\theta_c = 1^o$.

results in a fixed interpulse error. The shape of the error curves at these additional frequencies remains the same, but the peak error and optimum compensation angle increase with increasing resonant frequency.

At each frequency, error curves with 0.1^{o} resolution in θ_c were plotted, and the optimum angle was selected. Optimum pulse width error curves are plotted in Fig. 5. The resulting peak error and optimum angle are plotted against frequency in Figs. 6 and 7 respectively. Linearity of the optimum compensation angle plot implies an optimum compensation time measured from the peak of the waveform which is essentially independent of the frequency over the range considered. A linear fit to the plotted curve results in an optimum compensation delay of 0.5556 μsec.

C. Error for Constant R

The above procedure was repeated with R held constant at 5000 ohms to simulate a preamplifier having a fixed input resistance; L was held constant at 28 mH. The smaller capacitance at the higher frequencies (Eq. (17)) results in a shorter damping time constant and a smaller interpulse error than at 5.25 kHz. At each frequency, error curves and optimum angles were again computed and plotted in Figs. 6 and 7, using the value of C from Eq. (17). The results are quite similar to those obtained for 2RC = constant. In fact, the optimum angle curve cannot be distinguished within plotting errors from the case of fixed 2RC.

These results indicate that the dominating parameters in the pulse width error are ω_0, T, and the compensation time, $t_s - t_p$.

D. Error for an Impulse Charge

Having determined the peak error and optimum measurement time for an ideal rectangular current pulse ranging in width from 0 to 2 μsec, one may investigate the error for another form of charge distribution when operating at the previously determined optimum measurement point. In particular an impulse occurring at time t_0 (t_0 ranges from 0 to 2 μsec) was selected as a limiting case for the charge distribution.

The response of the resonant toroid to an impulse of current at $t_0 = 0$ has already been calculated in Section IV and the result is given in Eq. (9). The response for an input of a shifted current impulse becomes:

$$e_s = \frac{Qe^{-(t_s-t_0)/2RC}}{NC}\left[\cos\omega_0(t_s-t_0) - \frac{1}{2RC\,\omega_0}\sin\omega_0(t_s-t_0)\right] u(t_s-t_0) \quad (18)$$

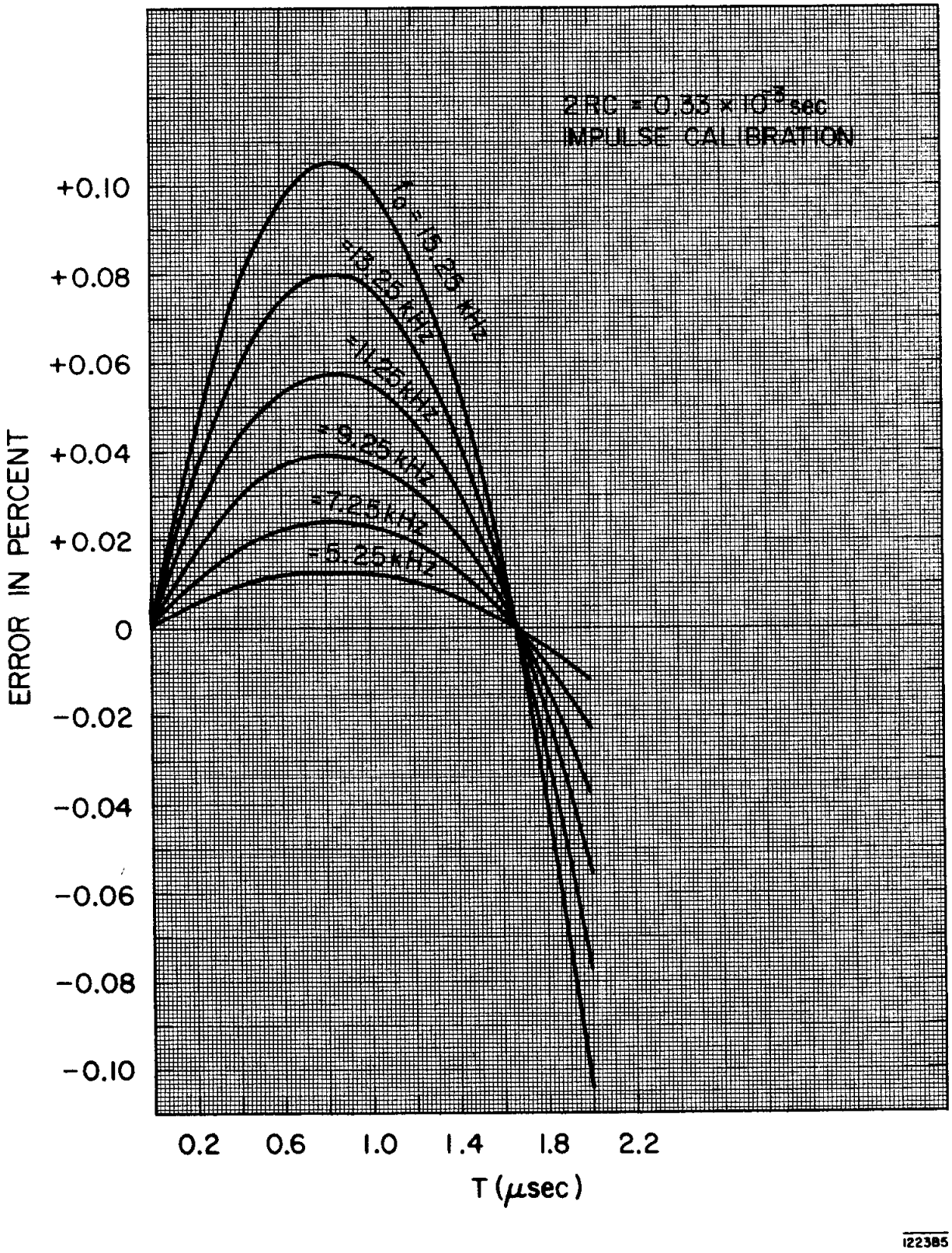

FIG. 5--Optimum pulse width error at selected frequencies, 2RC constant.

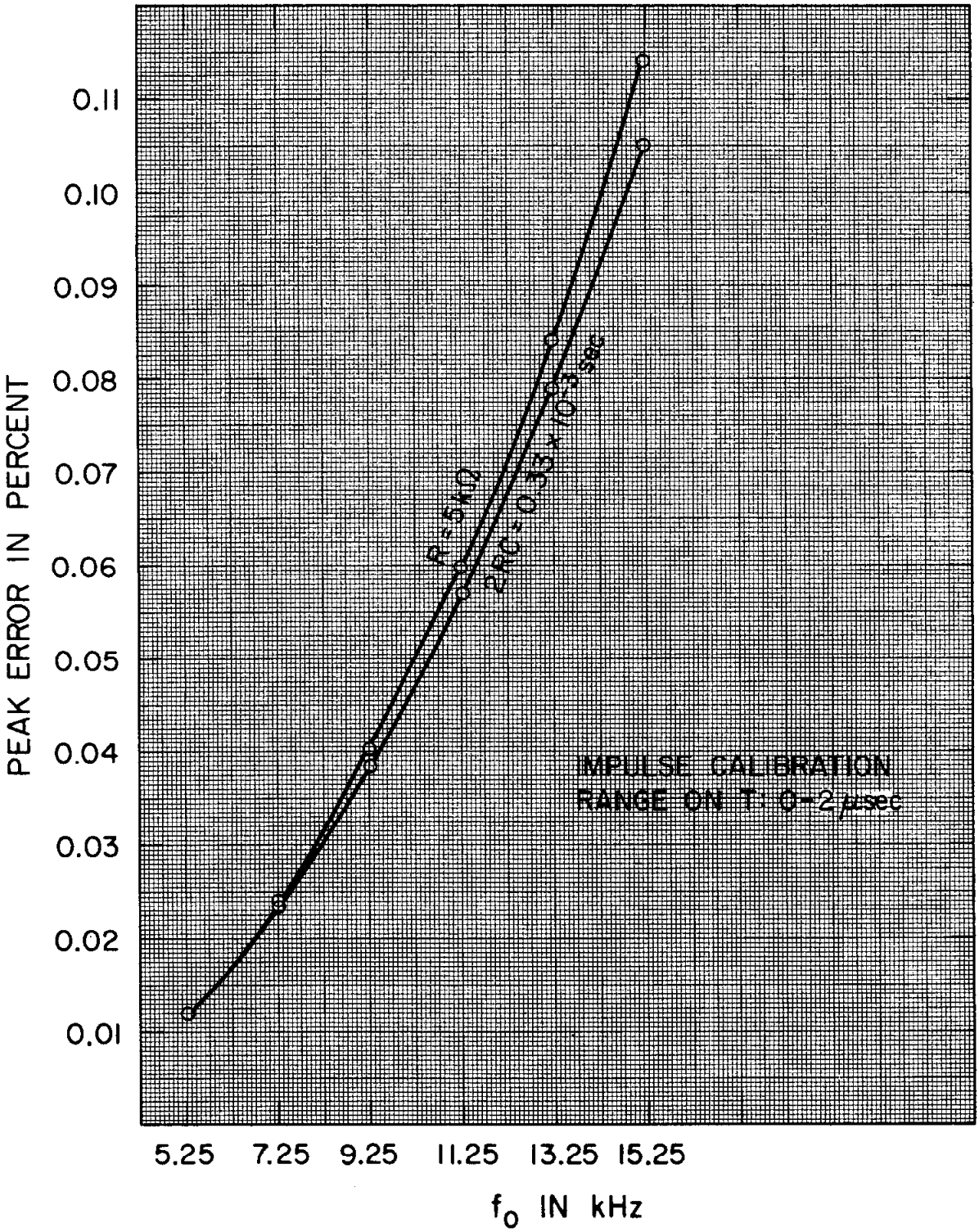

FIG. 6--Peak pulse width error over the range 5.25 kHz to 15.25 kHz, at the optimum θ_c.

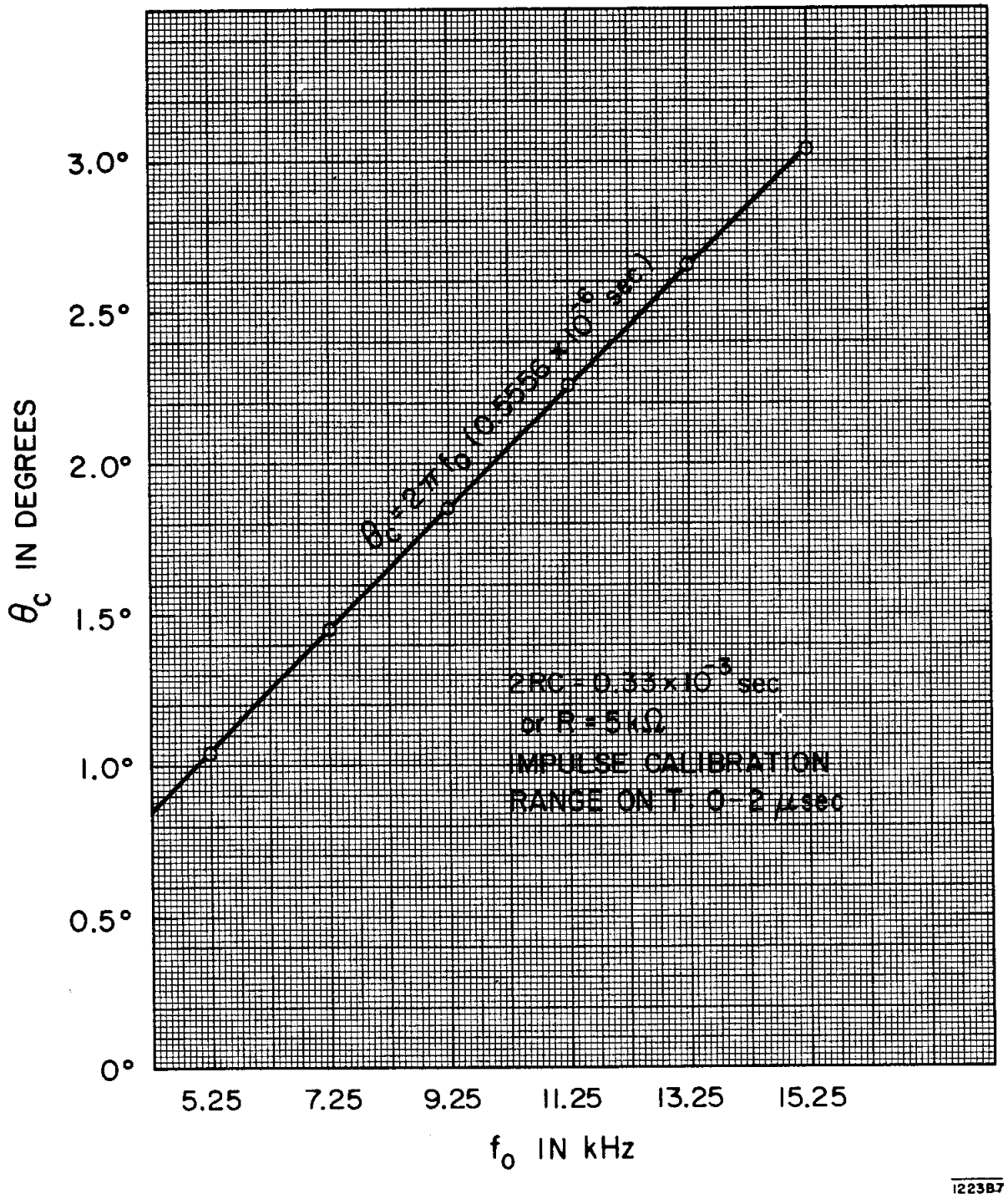

FIG. 7--Optimum compensation angle, over the range 5.25 kHz to 15.25 kHz.

Assuming impulse charge calibration at t = 0 and substituting Eq. (10) into Eq. (18) yields

$$e_s = Qe^{t_0/2RC}\,\frac{(e_s)_{cal}}{Q_{cal}}\,\frac{\left[\cos\omega_0(t_s-t_0) - \frac{1}{2RC\,\omega_0}\sin\omega_0(t_s-t_0)\right]}{\left[\cos\omega_0 t_s - \frac{1}{2RC\,\omega_0}\sin\omega_0 t_s\right]} \qquad (19)$$

Defining the impulse charge error as

$$\text{Error} = \frac{Q_{measured}}{Q} - 1 \qquad (20)$$

results in

$$\text{Error} = e^{t_0/2RC}\,\frac{\left[\cos\omega_0(t_s-t_0) - \frac{1}{2RC\,\omega_0}\sin\omega_0(t_s-t_0)\right]}{\left[\cos\omega_0 t_s - \frac{1}{2RC\,\omega_0}\sin\omega_0 t_s\right]} - 1 \qquad (21)$$

The resulting error curves for an impulse charge are plotted in Fig. 8, for the same resonant frequencies, with 2RC = 0.330 msec and with θ_c at the optimum compensation angle as previously determined. These curves show a similar shape to those for a rectangular pulse input, but indicate greater error, although the maximum error at 5.25 kHz is still less than 0.1 percent. Note that all of the error curves intersect the zero error axis in the vicinity of $t_0 = 1.15\ \mu$sec.

E. Error for a Rectangular Calibration Pulse

From the previously calculated results (Section VI.B) it is possible to compute the pulse width error for a more realistic calibration pulse, in particular a rectangular calibration pulse of width t_c, with known charge Q_{cal}. A value of $t_c = 0.5\ \mu$sec will be used for the computations. From Eq. (8) the response for a rectangular pulse of width t_c is

$$e_s = \frac{Q}{NC\,\omega_0 t_c}\,e^{-t_s/2RC}\left[\sin\omega_0 t_s - e^{t_c/2RC}\sin\omega_0(t_s-t_c)\right] \qquad (23)$$

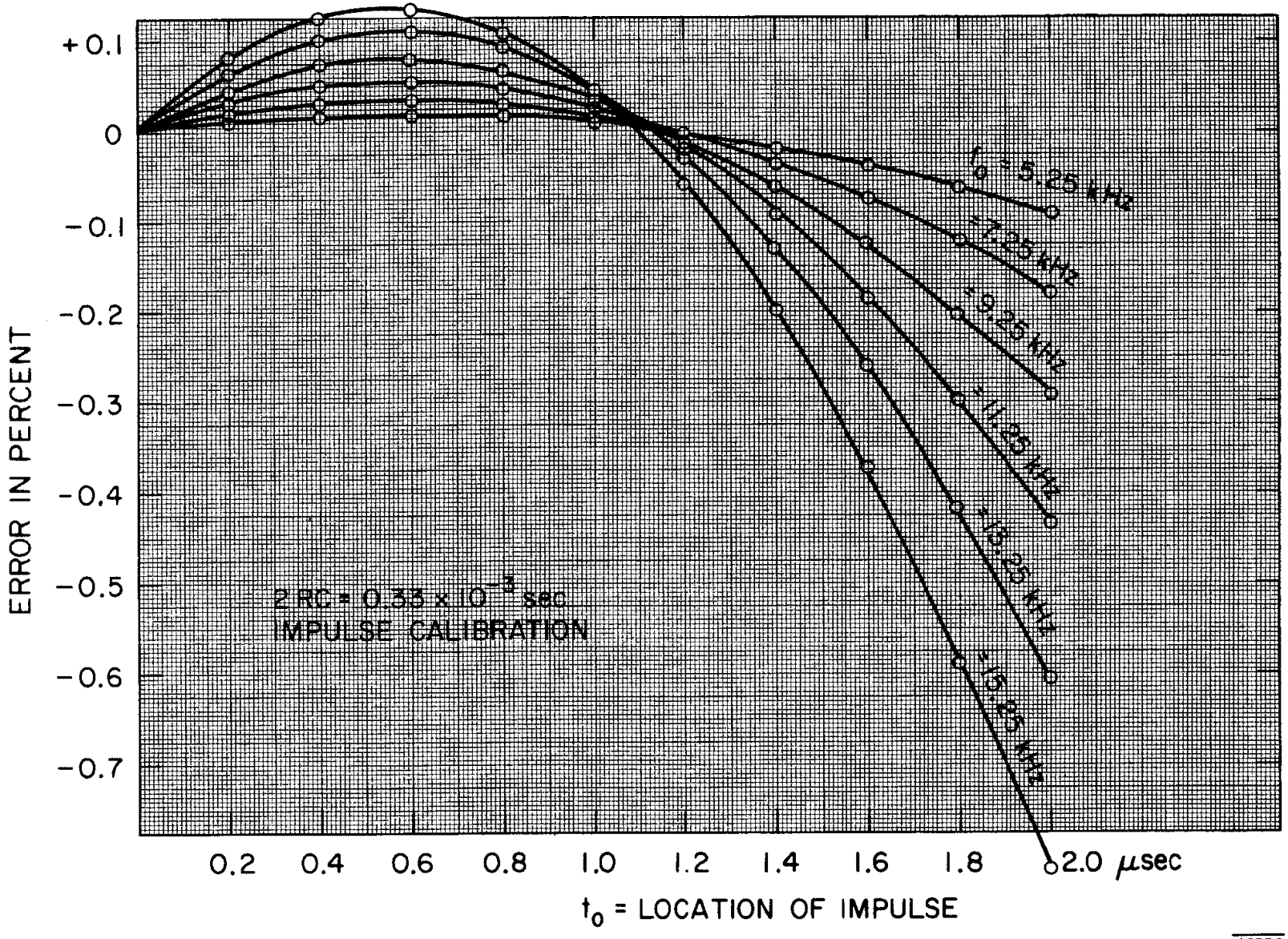

FIG. 8--Impulse charge error at optimum θ_c for selected frequencies.

Assuming that this is the calibration condition,

$$\frac{e^{-t_s/2RC}}{NC\,\omega_0} = \frac{(e_s)_{cal}}{Q_{cal}} \quad \frac{t_c}{\sin \omega_0 t_s - e^{t_c/2RC} \sin \omega_0 (t_s - t_c)} \tag{24}$$

Substituting into Eq. (8),

$$e_s = Q \frac{t_c}{T} \frac{(e_s)_{cal}}{Q_{cal}} \frac{\sin \omega_0 t_s - e^{T/2RC} \sin \omega_0 (t_s - T)}{\sin \omega_0 t_s - e^{t_c/2RC} \sin \omega_0 (t_s - t_c)} \tag{25}$$

If the error is again defined as $\frac{Q_{meas} - Q}{Q}$ then

$$E_r = \frac{t_c}{T} \frac{\left[\sin \omega_0 t_s - e^{T/2RC} \sin \omega_0 (t_s - T)\right]}{\left[\sin \omega_0 t_s - e^{t_c/2RC} \sin \omega_0 (t_s - t_c)\right]} - 1 \tag{26}$$

This error is defined as the rectangular calibration error E_r, referring to the assumed shape of the calibration pulse. For a fixed t_c, t_s, ω_0, and 2RC the error can be written as

$$E_r = K_1 \frac{\sin \omega_0 t_s - e^{T/2RC} \sin \omega_0 (t_s - T)}{T} - 1 \tag{27}$$

For an impulse calibration (Section IV) the pulse width error (Eq. (13)) for a fixed ω_0, t_s, and 2RC can be written as

$$E_i = K_2 \frac{\sin \omega_0 t_s - e^{T/2RC} \sin \omega_0 (t_s - T)}{T} - 1 \tag{28}$$

Therefore for a given T,

$$\frac{1 + E_r}{1 + E_i} = \frac{K_1}{K_2} = K_3 \tag{29}$$

or

$$1 + E_r = K_3 (1 + E_i) .$$

The constant K_3 is determined by the impulse error at $T = t_c$, since the rectangular calibration error must be zero when the beam width T equals the calibration width t_c.

Therefore

$$1+E_r(T) = \frac{1 + E_i(T)}{1+E_i(t_c)} \tag{30}$$

As a result, the previously calculated error curves for impulse calibration (Figs. 3 and 4) can be used to find the error curves for a rectangular calibration pulse. For small errors it can be shown that

$$E_r(T) \cong E_i(T) - E_i(t_c) \tag{31}$$

with a calculation error approximately equal to the impulse calibration error at $T = t_c$. Thus, the rectangular calibration error calculations given by Eq. (31) are accurate to better than 1%, for impulse calibration errors below 1%.

However, an error curve so generated is associated with a different compensation angle from the impulse calibration error curve, since the reference peak of the waveform shifts for a rectangular calibration pulse. The correction is found by differentiating Eq. (23) and setting the result equal to zero, in order to find the location of the new peak.

$$\frac{de_s}{dt_s} = \frac{Qe^{-\frac{t_s}{2RC}}}{NC\,\omega_0 t_c}\left\{\left[\omega_0 \cos \omega_0 t_s - e^{t_c/2RC}\,\omega_0 \cos \omega_0(t_s-t_c)\right]\right.$$
$$\left. - \frac{1}{2RC}\left[\sin \omega_0 t_s - e^{t_c/2RC}\,\sin \omega_0(t_s-t_c)\right]\right\} = 0 \tag{32}$$

Solution of Eq. (32) yields the following result for the time of the peak:

$$t_p = \frac{1}{\omega_0} \arctan \frac{e^{t_c/2RC}\left(\cos \omega_0 t_c + \frac{1}{2RC\,\omega_0} \sin \omega_0 t_c\right) - 1}{-e^{t_c/2RC}\left(\sin \omega_0 t_c - \frac{1}{2RC\,\omega_0} \cos \omega_0 t_c\right) - \frac{1}{2RC\,\omega_0}} \tag{33}$$

where $\frac{\pi}{2} < \omega_0 t_p < \frac{3\pi}{2}$ and t_p is in seconds. For $2RC = 0.33 \times 10^{-3}$ sec., $t_c = 0.5 \times 10^{-6}$ sec and $\omega_0 = 2\pi \times 5.25 \times 10^3$ sec^{-1} ... 15.25×10^3 sec^{-1} the shift in t_p is shown in Table I. Note that the change in t_p is very close to one-half the calibration pulse width.

Shifting the original error data according to Eq. (31) and using the data in Table 1 to correct the compensation angle, the new error curves are plotted in Fig. 9. The optimum compensation angle, defined again as that which minimizes the peak error, is about 0.8° compared to the optimum compensation angle of 1.05° for impulse calibration. The resulting peak error of .014% is slightly greater than the peak error for impulse calibration (.012%).

A similar procedure followed for the remaining frequencies results in an optimum angle which is again linear with frequency, corresponding to a fixed compensation time of 0.417 μsec. This is a shift in optimum compensation of .138 μsec from that of impulse calibration (see Section VI.B). The increase in peak error is less than 15% over the peak error for impulse calibration.

VII. TIMING ERROR ANALYSIS

In the previous sections, charge measurement errors due to changes in charge distribution have been discussed. It is also possible to analyse errors due to measurement time changes. The timing change can take place in either of two areas: (1) A change in t_s due to instabilities of timing within the charge measurement system. (2) A change in the beam pretrigger reference timing $t = 0$ with respect to the beam pulse leading edge. The error analysis which follows applies equally well to either type of timing error.

The method of analysis will be to differentiate the expression for e_s (Eq. (8)) resulting in the slope of the waveform in volts/sec. Then dividing by the value of e_s at that point gives the relative timing error. Substituting the optimum compensation angle gives the timing error variation with pulse width T when operating at the optimum point for a rectangular input pulse.

Performing the operations above, and rearranging terms yields

$$\frac{de_s}{dt_s} \Big/ e_s = \left[\omega_0 \frac{\cos \omega_0 t_s - e^{T/2RC} \cos \omega_0 (t_s - T)}{\sin \omega_0 t_s - e^{T/2RC} \sin \omega_0 (t_s - T)} - \frac{1}{2RC} \right] \times 10^{-6},$$

which gives the relative slope per microsecond.

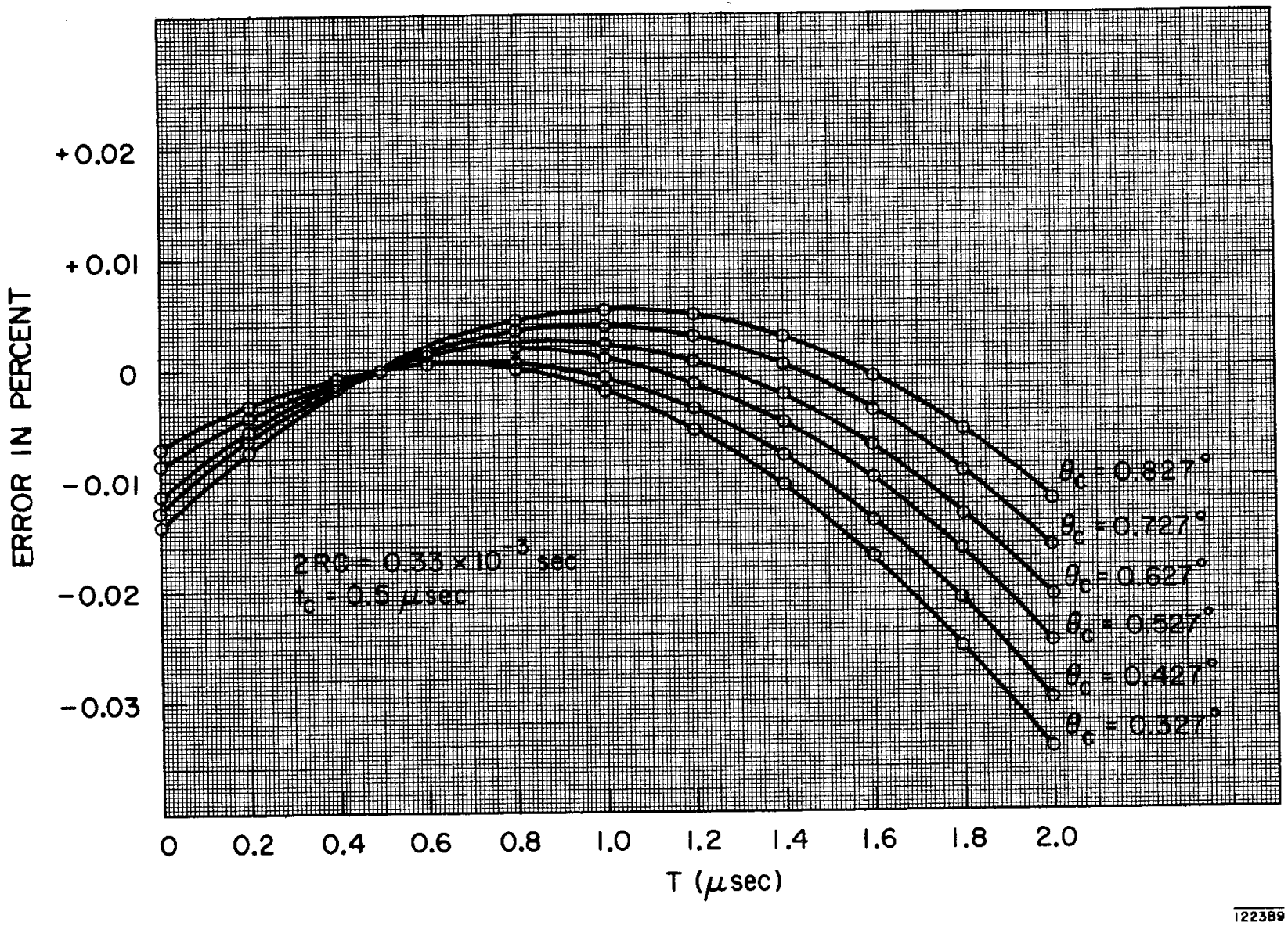

FIG. 9--Pulse width error at 5.25 kHz for rectangular calibration of width 0.5 μsec.

Using the previous set of values for resonant frequency, holding 2RC constant at .330 msec, and ranging T from 0 to 2 μsec, the timing error function was calculated and is plotted in Fig. 10.

Note that operation at the optimum compensation angle essentially minimizes the peak timing error. An error curve for a compensation angle of 0^{o} is included to demonstrate this point. Note also that the timing error or waveform slope is zero at about T = 1.13 μsec, indicating operation at the peak of the waveform for this value of T.

At 5.25 kHz the maximum timing error is about .07 percent per microsecond.

VIII. SUMMARY AND CONCLUSIONS

The major results of the analysis and calculations for a 0-2 μsec beam can be summarized as follows:

a. At a resonant frequency of 5.25 kHz and a range in pulse width of 0 - 2 μsec, a compensation angle of $\theta_c = 1.05^{o}$ minimizes the peak pulse width error to ± .012%. If no compensation is used the peak error is - .073%.

b. At higher frequencies, with 2RC constant at .33 msec, the optimum compensation time (0.5556 μsec) is independent of frequency up to 15.25 kHz. The optimum peak error increases with frequency; at 15.25 kHz it is ± .105%.

c. With R held constant at 5000 ohms, the result is similar to (b) but with slightly greater peak error at the higher frequencies.

d. With the system optimized for a 0 - 2 μsec pulse, the peak error for an impulse charge input over the same range approaches 0.1% at 5.25 kHz, and 0.85% at 15.25 kHz.

e. The use of a 0.5 μsec rectangular calibration pulse instead of an impulse results in a .138 μsec shift in the optimum compensation time, and approximately a 15% increase in the peak error.

f. The optimum compensation angle, which minimizes the peak pulse width error, also tends to minimize the peak timing error slope.

g. The timing error slope increases with resonant frequency; the worst slope is about -.07%/μsec at 5.25 kHz, and about - 0.5%/μsec at 15.25 kHz. The timing error curves indicate a waveform slope of zero for a pulse width of 1.13 μsec, independent of frequency.

Several other conclusions concerning system design and performance are possible. First, assuming that the system is always in calibration, then the error due to a slow resonant frequency change is given by the slope of Fig. 6, which is 0.0003% for a 1% change in frequency at 5.25 kHz. It may also be concluded that slow variations in the time constant 2RC have little effect on the error.

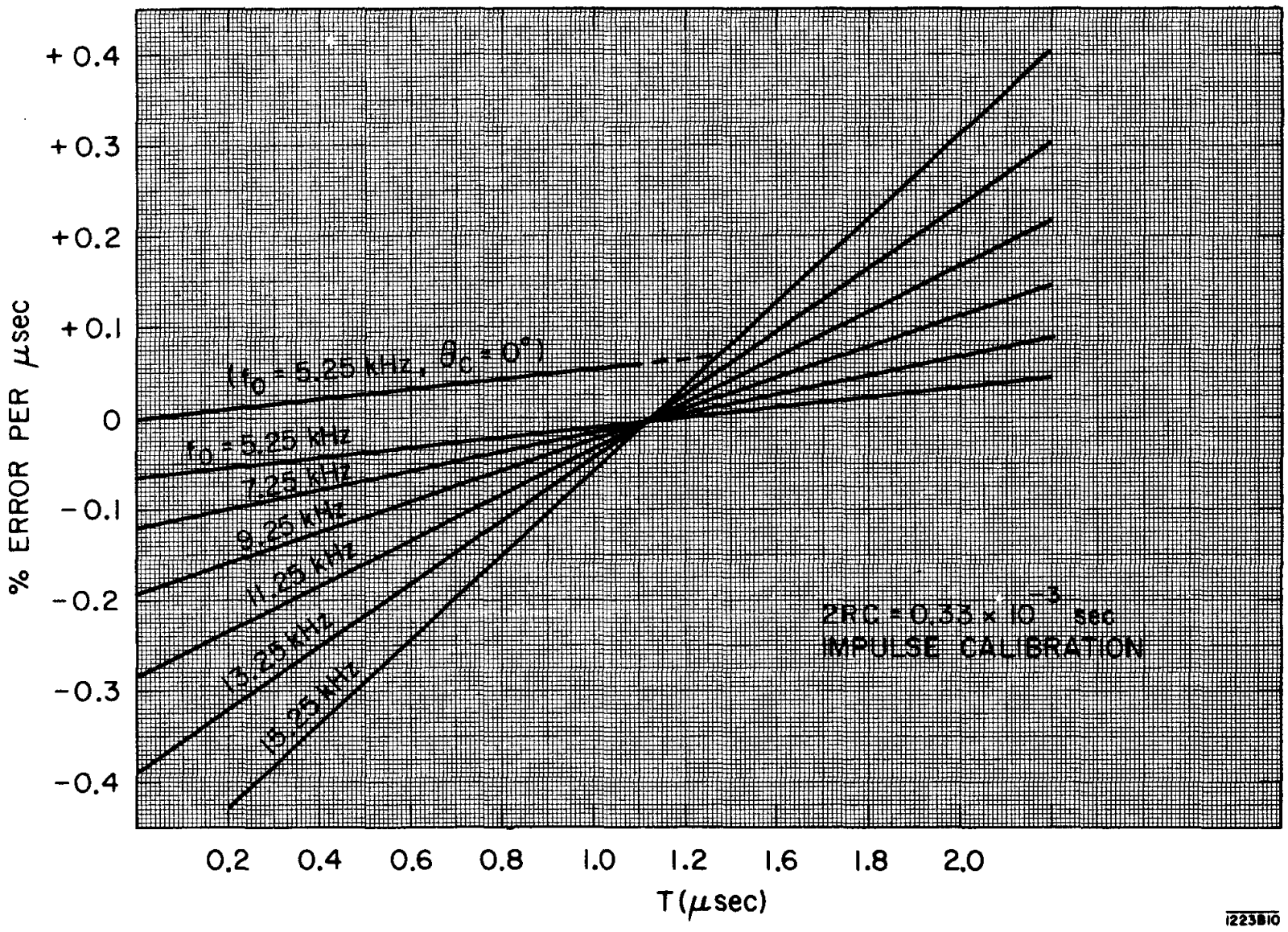

FIG. 10--Timing error at optimum θ_c for selected frequencies.

The result (b) above, that the optimum angle corresponds to a fixed compensation time, implies that the system can be constructed with a fixed compensation time,thereby simplifying the electronic circuits.

It has been shown that the peak error for finite width calibration (0.5 μsec) is somewhat greater than that for impulse calibration. From the nature of the error curves it is apparent that the use of impulse calibration minimizes the peak error. On this basis the calibrator should be designed to have the smallest possible pulse width.

It should be recognized that there are other factors contributing to the overall accuracy of a resonant toroid charge monitor system. Some of the more important ones are listed below.

1. Imperfections in the electronics (amplifiers, etc.)
2. Imperfections in the toroid model
3. Accuracy of the calibration charge
4. Precision of system adjustment
5. Drifts in system parameters after calibration
6. Effects of system noise

The latter factor is quite important, since the toroid signal may be in the microvolt region. It should be noted that the toroid signal increases for higher frequencies so that increased pulse width and timing errors can be traded against improved signal-to-noise ratio.

REFERENCES

1. R. S. Larsen and D. Horelick, "A precision toroidal charge monitor for SLAC," Symposium on Beam Intensity Measurement-Proceedings, V. W. Hatton and S. Lowndes, Editors, SRC (1968); p. 260-279.
2. J. T. Hyman, "Toroidal transformers and preamplifiers for transparent beam-current monitors," Report No. N1RL/R/30, Rutherford High Energy Laboratory (March 1963).
3. Thanh Khai Truong, "Intégration Coup par Coup de Faisceau d'un Accélérateur Pulsé," Thesis, Faculté des Sciences, École Normale Supérieure, Laboratoire de l'Accélérateur Linéaire, Orsay, France (1967).
4. D. B. Isabelle, "Beam current monitors for a high energy linac," Report No. SLAC-25-C, Stanford Linear Accelerator Center, Stanford University, Stanford, California (1963); p. 46.